JOURNAL OF THERMOPHYSICS AND HEAT TRANSFER
Vol. 14, No. 4, October–December 2000

Natural Convection Simulation Inside the Underground Conduit of an Electrical Power Cable

Chun-Lang Yeh*
National Huwei Institute of Technology, Huwei, Yunlin 632, Taiwan, Republic of China
and
Keh-Chin Chang†
National Cheng-Kung University, Tainan 701, Taiwan, Republic of China

The heat dissipation process inside a power cable conduit buried underground is characterized by the three-dimensional natural convection between horizontal, highly eccentric cylinders. The surface of the outer cylinder (concrete conduit) is assumed adiabatic, whereas a constant heat flux, representing heat generation from the power cable due to electrical resistance, is specified on the surface of the inner cylinder (power cable). Unlike the vertical configuration of eccentric annuli in which the fully developed thermal boundary conditions may be achievable, the boundary conditions at the open end of the present case are troublesome and are coped with by the zonal grid approach. Two cases with the modified Rayleigh numbers of 10^5 and 10^6 are investigated. A numerical study reveals that cable surface temperatures increase toward the outlet plane. It is also found that higher temperatures occur in the region near the bottom of the inner cylinder, where the cable contacts the concrete conduit (outer cylinder), due to small local Rayleigh numbers in which the characteristic length is defined in terms of radial distance between the inner and outer cylinders. As a result, the portion of the power cable near the contacting point with the concrete conduit will deteriorate earlier.

Nomenclature

C_p	=	specific heat capacity
D_h	=	hydraulic diameter
Ec	=	Eckert number, $V^{*2}/C^*_{p\,\mathrm{ref}} q^*_w D^*_h / k^*_{\mathrm{ref}}$
Fr	=	Froude number, $V^*/\sqrt{(g^* D^*_h)}$
Gr	=	Grashof number, Ra/Pr
g	=	gravitational acceleration
g^{jk}	=	contravariant metric tensor
h	=	convective heat transfer coefficient
J	=	Jacobian
k	=	thermal conductivity
l	=	radial distance between the inner and outer cylinders
Nu	=	Nusselt number, $h^* D^*_h / k^*_{\mathrm{ref}}$
Pr	=	Prandtl number, υ^*/α^*
p	=	hydraulic pressure, $(p^* + \rho^*_{\mathrm{ref}} g^* y^*)/\rho^*_{\mathrm{ref}} V^{*2}$
q	=	heat flux
q^j	=	curvilinear coordinate
R^Φ	=	source term
Ra	=	Rayleigh number, $g^*\beta^* D^{*3}_h \Delta T^*/\upsilon^*\alpha^*$
Ra^0	=	modified Rayleigh number, $g^*\beta^* D^{*4}_h q^*_w/\upsilon^*\alpha^* k^*$
T	=	temperature
(u, v, w)	=	physical velocity, $(u^*, v^*, w^*)/V^*$
V^j	=	contravariant velocity
V^*	=	characteristic velocity, α^*/D^*_h
(x, y, z)	=	Cartesian coordinates, $(x^*, y^*, z^*)/D^*_h$
α	=	thermal diffusivity
β	=	thermal expansion coefficient
Γ^Φ	=	diffusion coefficient
θ	=	nondimensionalized temperature, $(T^* - T^*_{\mathrm{ref}})/(q^*_w D^*_h/k^*)$
μ	=	viscosity
ρ	=	density, $\rho^*/\rho^*_{\mathrm{ref}}$
υ	=	kinematic viscosity
Φ	=	energy dissipation term, also dependent variable
ϕ	=	azimuthal angle

Subscripts

b	=	bulk
i	=	inner cylinder
l	=	local
nb	=	neighboring grid points
o	=	outer cylinder
P	=	main grid point
ref	=	reference state (at atmospheric pressure and room temperature)
w	=	wall

Superscripts

—	=	averaged quantity
*	=	dimensional quantity

Introduction

PLACING power cables underground is an engineering tendency nowadays, especially in city areas and industrial zones, due to limited available space. The power cable (inner cylinder) is placed inside a concrete conduit (outer cylinder) buried underground and lies on the bottom of the conduit. The configuration of this layout is an annulus between two horizontal, highly eccentric cylinders. Heat is generated from the electrical resistance of the power cable and the heat dissipation process in the annulus relies on the natural convection heat transfer from both open ends of the conduit, which penetrate onto the manhole surfaces. The heat dissipation rate in the annulus is important because it will affect the lifetime of the power cable. The heat dissipation rate is determined from the ventilation stemmed from natural convection. Thus, under a situation of bad ventilation in the underground conduit, the power cable will deteriorate earlier than its designed usage time.

The computational domain is schematically shown in Fig. 1, with the symmetric nature of the flowfield with respect to the two open ends and to a vertical plane crossing the center of the cylinders taken into account. In addition to the convection heat transfer, a more comprehensive thermal model for the configuration investigated should

Received 23 September 1999; revision received 22 February 2000; accepted for publication 29 February 2000.

*Assistant Professor, Department of Aeronautical Engineering; clyeh@sunws.nhit.edu.tw.
†Professor, Department of Aeronautics and Astronautics.

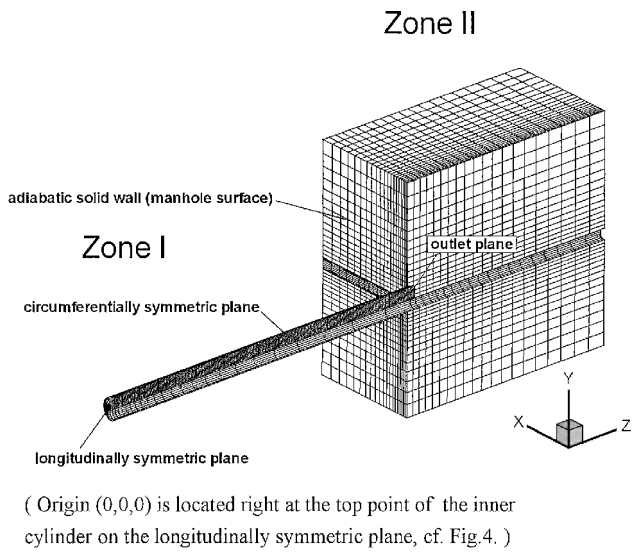

Fig. 1 Illustration of the computational domain and zonal grid distribution.

include the thermal radiation inside the enclosure and the thermal conduction along the cable and the concrete wall. However, the present study is focused on the convection problem only. The additional complication due to the consideration of thermal radiation in the enclosure and thermal conduction along the cable, as well as the concrete wall, is reserved for future study. The boundary conditions for this problem are as follows. The adiabatic condition is given on the outer cylinder (concrete conduit) surface, whereas on the inner cylinder (power cable), a constant heat flux, which is specified with the heat generation from the power cable due to electrical resistance, is given. A no-slip condition is given to the three components of the velocity on the outer and inner cylinder surfaces. Because no flow crosses the circumferentially (or longitudinally) symmetric plane, the angular (or axial) velocity vanishes on that plane. The angular (or axial) derivatives of the remaining velocity components and temperature also vanish on the circumferentially (or longitudinally) symmetric plane. Unlike the vertical configuration of eccentric annuli in which the fully developed thermal boundary conditions may be achievable,[1] the boundary conditions at the open end of the present case are troublesome and will be elaborated on later. Although this plane is named as the outlet (see Fig. 1) in consideration of the heat dissipation route in the conduit, it consists of inflow and outflow at the same plane (see Fig. 2).

Many theoretical and experimental studies on natural convection in horizontal, eccentric annuli have been carried out. In most of these studies, a two-dimensional model was used in which the annuli are assumed to be infinitely long and coupled with thermal boundary conditions on the cylinder surfaces specified, either with two constant wall temperatures or one with a constant wall temperature and the other with a constant wall heat flux (including adiabatic surface).[2–10] A typical example is the numerical work of Ho and Lin.[2] In their work, a steady natural convection flow of gases between two horizontal cylinders, which were maintained at two constant temperatures, was studied. Moreover, Glakpe et al.[11] numerically investigated the steady two-dimensional natural convection between concentric and eccentric horizontal cylinders with specified (constant) heat flux at the boundaries. Within the content of experimental studies, Kuehn and Goldstein[4,7,8] were among the earlier researchers who investigated natural convection within concentric and eccentric annuli. In their study,[7] the Rayleigh number Ra ranges from 10^3 to 10^8, which covers regions of conduction as well as laminar and turbulent convection. It was found that periodic fluctuation of the upper-half of the outer cylinder occurs near $Ra = 4 \times 10^6$, signifying an onset of transition. As the Rayleigh number is further increased up to 5×10^8, the complete upper portion of the annuli is turbulent. In contrast, the area apart from the intensified fluctuation region remains steady where viscous and conduction effects, in terms of flow and thermal fields, respectively, are predominant. However, the boundary conditions on the cylinder surfaces do not permit the steady-state solution of a two-dimensional natural convection within the transverse plane in the present work. Three-dimensional formulation has to be used to model the problem. There have been few three-dimensional investigations of natural convection in concentric annuli between two horizontal cylinders, except with a cavity-type configuration.[12–15] A comprehensive literature survey has revealed that published work is largely nonexistent on three-dimensional eccentric annuli between two horizontal cylinders, where their geometric configurations possess open ends (not an annular cavity). The scope of this work is to investigate numerically the flow and thermal fields of laminar natural convection in the geometric configuration schematically shown in Fig. 1.

The flow pattern of interest here necessitates the solutions of three-dimensional, fully elliptic type of partial differential equations. As mentioned before, selection of the proper boundary conditions at the outlet plane is a major issue to be addressed in the work. An approach frequently used in the simulations of the noncavity type, buoyancy-induced flows is the zonal grid approach,[16,17] which extends the computational domain outside the outlet plane so that the boundary conditions can be reasonably specified with the ambient flow properties. Typical examples can be found in Refs. 18–20. Although this approach requires enormous computations for three-dimensional problems, it provides more reliable results among existing approaches. An alternative but greatly economical approximation, as made in Ref. 21, is to assume the flow to be longitudinally parabolic after it travels a long enough axial distance in the flowfield. In other words, neither momentum nor heat is diffused in the axial direction, and it then permits a marching-integration calculation procedure in numerical analysis. However, this parabolic approximation requires that the flow possess a predominant flow direction, which is obviously inconsistent with the present problem. In this work, the zonal grid approach is adopted to resolve the problem of the outlet boundary conditions.

Mathematical Model

The flow pattern of interest here necessitates the solution of three-dimensional, fully elliptic type of partial differential equations, which describe the natural convection flowfield. Considering the steady-state flow situation, the nondimensionalized governing equations in Cartesian coordinates read

$$\frac{\partial}{\partial x}(\rho u) + \frac{\partial}{\partial y}(\rho v) + \frac{\partial}{\partial z}(\rho w) = 0 \tag{1}$$

$$\frac{\partial}{\partial x}(\rho uu) + \frac{\partial}{\partial y}(\rho vu) + \frac{\partial}{\partial z}(\rho wu) = -\frac{\partial p}{\partial x} + Pr \cdot \left[\frac{\partial^2 u}{\partial x^2} + \frac{\partial^2 u}{\partial y^2} + \frac{\partial^2 u}{\partial z^2} + \frac{1}{3}\frac{\partial}{\partial x}\left(\frac{\partial u}{\partial x} + \frac{\partial v}{\partial y} + \frac{\partial w}{\partial z}\right)\right] \tag{2}$$

$$\frac{\partial}{\partial x}(\rho uv) + \frac{\partial}{\partial y}(\rho vv) + \frac{\partial}{\partial z}(\rho wv) = -\frac{\partial p}{\partial y} + Pr \cdot \left[\frac{\partial^2 v}{\partial x^2} + \frac{\partial^2 v}{\partial y^2} + \frac{\partial^2 v}{\partial z^2} + \frac{1}{3}\frac{\partial}{\partial y}\left(\frac{\partial u}{\partial x} + \frac{\partial v}{\partial y} + \frac{\partial w}{\partial z}\right)\right] - \frac{1-\rho}{Fr^2} \tag{3}$$

$$\frac{\partial}{\partial x}(\rho uw) + \frac{\partial}{\partial y}(\rho vw) + \frac{\partial}{\partial z}(\rho ww) = -\frac{\partial p}{\partial z} + Pr \cdot \left[\frac{\partial^2 w}{\partial x^2} + \frac{\partial^2 w}{\partial y^2} + \frac{\partial^2 w}{\partial z^2} + \frac{1}{3}\frac{\partial}{\partial z}\left(\frac{\partial u}{\partial x} + \frac{\partial v}{\partial y} + \frac{\partial w}{\partial z}\right)\right] \tag{4}$$

$Ra^o = 10^5$

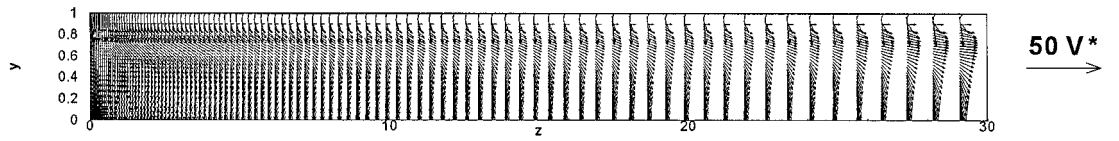

Cross section A-A

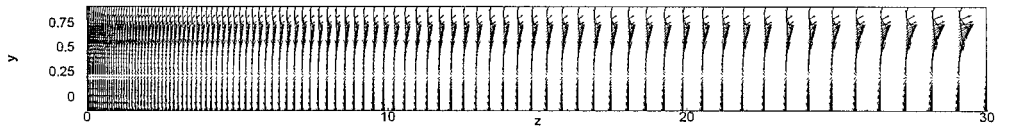

Cross section B-B

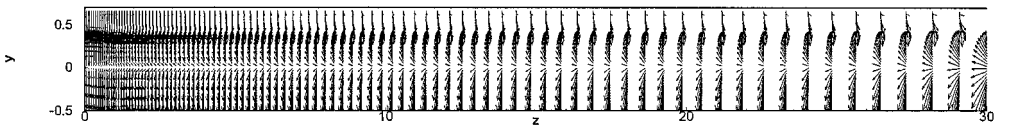

Cross section C-C

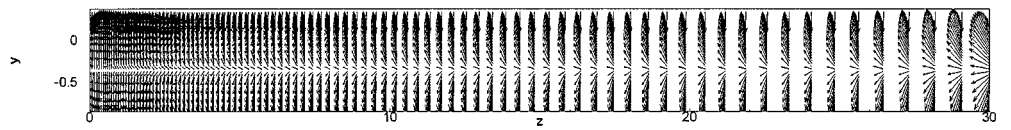

Cross section D-D

$Ra^o = 10^6$

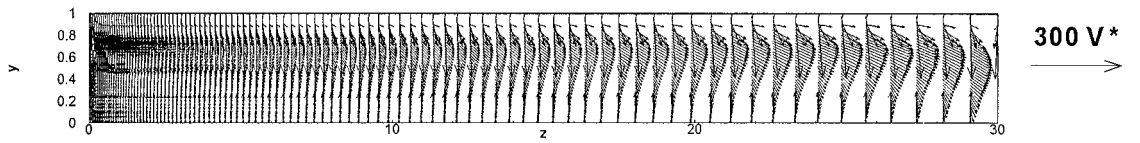

Cross section A-A

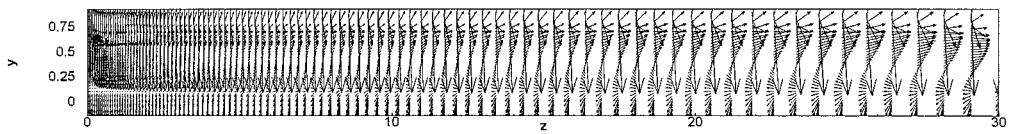

Cross section B-B

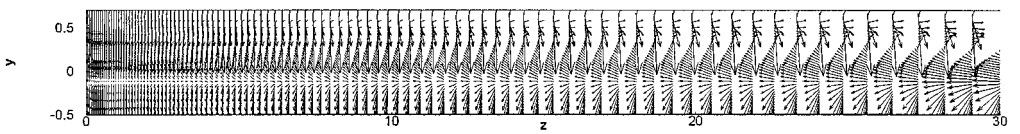

Cross section C-C

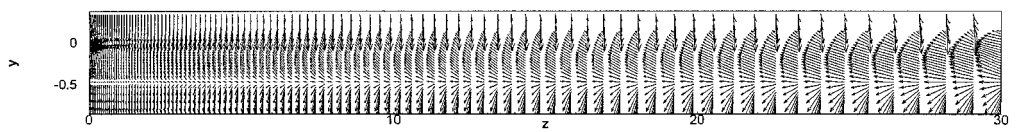

Cross section D-D

Fig. 2 Velocity vector plots at four longitudinal sections.

$$\frac{\partial}{\partial x}(\rho u\theta) + \frac{\partial}{\partial y}(\rho v\theta) + \frac{\partial}{\partial z}(\rho w\theta) = \frac{\partial^2\theta}{\partial x^2} + \frac{\partial^2\theta}{\partial y^2} + \frac{\partial^2\theta}{\partial z^2} + Ec\cdot\left(u\frac{\partial p}{\partial x} + v\frac{\partial p}{\partial y} + w\frac{\partial p}{\partial z}\right) + Pr\cdot Ec\cdot\Phi - \Pi \tag{5}$$

where

$$\Phi = 2\left[\left(\frac{\partial u}{\partial x}\right)^2 + \left(\frac{\partial v}{\partial y}\right)^2 + \left(\frac{\partial w}{\partial z}\right)^2\right] + \left(\frac{\partial u}{\partial y} + \frac{\partial v}{\partial x}\right)^2 + \left(\frac{\partial u}{\partial z} + \frac{\partial w}{\partial x}\right)^2 + \left(\frac{\partial v}{\partial z} + \frac{\partial w}{\partial y}\right)^2 - \frac{2}{3}\left(\frac{\partial u}{\partial x} + \frac{\partial v}{\partial y} + \frac{\partial w}{\partial z}\right)^2 \tag{6}$$

$$\Pi = \mu^* V^* g^* \Big/ q_w^* \tag{7}$$

Note that the Boussinesq approximation usually made in the formulation of natural convection is not adopted here and that the density is determined using the ideal gas law.

Numerical Method

The preceding governing equations can be cast into the following general form, which permits a single algorithm to be used:

$$\frac{\partial}{\partial x_j}(\rho v_j\Phi) = \frac{\partial}{\partial x_j}\left(\Gamma^\Phi\frac{\partial\Phi}{\partial x_j}\right) + R^\Phi \tag{8}$$

To facilitate handling of the complex geometry of the present problem, the body-fitted coordinate system is used to transform the physical domain into a computational domain, which is in a rectangular coordinate system with uniform control volumes. Transformation of Eq. (8) to the body-fitted coordinates leads to

$$\frac{\partial}{\partial q^j}(J\rho V^j\Phi) = \frac{\partial}{\partial q^j}\left(Jg^{jk}\Gamma^\Phi\frac{\partial\Phi}{\partial q^k}\right) + JR^\Phi \tag{9}$$

where q^j are curvilinear coordinates (ξ, η, ζ), J is the Jacobian identical to $x_\xi y_\eta z_\zeta + x_\eta y_\zeta z_\xi + x_\zeta y_\xi z_\eta - x_\zeta y_\eta z_\xi - x_\xi y_\zeta z_\eta - x_\eta y_\xi z_\zeta$, V^j is the contravariant velocity (U, V, W), where

$$U = (1/J)[u(y_\eta z_\zeta - y_\zeta z_\eta) + v(x_\zeta z_\eta - x_\eta z_\zeta) + w(x_\eta y_\zeta - x_\zeta y_\eta)]$$

$$V = (1/J)[u(y_\zeta z_\xi - y_\xi z_\zeta) + v(x_\xi z_\zeta - x_\zeta z_\xi) + w(x_\zeta y_\xi - x_\xi y_\zeta)]$$

$$W = (1/J)[u(y_\xi z_\eta - y_\eta z_\xi) + v(x_\eta z_\xi - x_\xi z_\eta) + w(x_\xi y_\eta - x_\eta y_\xi)]$$

and g^{jk} is the metric tensor, where

$$g^{11} = (1/J^2)\left[(y_\eta z_\zeta - y_\zeta z_\eta)^2 + (x_\zeta z_\eta - x_\eta z_\zeta)^2 + (x_\eta y_\zeta - x_\zeta y_\eta)^2\right]$$

$$g^{12} = g^{21} = (1/J^2)[(y_\eta z_\zeta - y_\zeta z_\eta)(y_\zeta z_\xi - y_\xi z_\zeta) + (x_\zeta z_\eta - x_\eta z_\zeta)(x_\xi z_\zeta - x_\zeta z_\xi) + (x_\eta y_\zeta - x_\zeta y_\eta)(x_\zeta y_\xi - x_\xi y_\zeta)]$$

$$g^{13} = g^{31} = (1/J^2)[(y_\eta z_\zeta - y_\zeta z_\eta)(y_\xi z_\eta - y_\eta z_\xi) + (x_\zeta z_\eta - x_\eta z_\zeta)(x_\eta z_\xi - x_\xi z_\eta) + (x_\eta y_\zeta - x_\zeta y_\eta)(x_\xi y_\eta - x_\eta y_\xi)]$$

$$g^{22} = (1/J^2)\left[(y_\zeta z_\xi - y_\xi z_\zeta)^2 + (x_\xi z_\zeta - x_\zeta z_\xi)^2 + (x_\zeta y_\xi - x_\xi y_\zeta)^2\right]$$

$$g^{23} = g^{32} = (1/J^2)[(y_\zeta z_\xi - y_\xi z_\zeta)(y_\xi z_\eta - y_\eta z_\xi) + (x_\xi z_\zeta - x_\zeta z_\xi)(x_\eta z_\xi - x_\xi z_\eta) + (x_\zeta y_\xi - x_\xi y_\zeta)(x_\xi y_\eta - x_\eta y_\xi)]$$

$$g^{33} = (1/J^2)\left[(y_\xi z_\eta - y_\eta z_\xi)^2 + (x_\eta z_\xi - x_\xi z_\eta)^2 + (x_\xi y_\eta - x_\eta y_\xi)^2\right]$$

In consideration of a highly eccentric configuration, the grid layout is constructed by connecting the grid points in each transverse plane, which are generated by solving the two-dimensional, elliptic type of partial differential equations governing the distribution of the grid points.[22] Numerical calculation of Eq. (9) is performed using the control-volume based finite difference procedure. The discretized governing equations are solved on a nonstaggered grid system in association with the SIMPLEC algorithm[23] and QUICK scheme.[24] In the use of the zonal grid approach,[16–20] the computational domain is extended outside the outlet plane and is divided into two subdomains of zones I and II, as schematically illustrated in Fig. 1. The inner and outer diameters of zone I are 0.1 and 0.2 m, respectively, while its length is equal to 3 m (equivalent to $30D_h^*$). Note that the conduit length between two consecutive manholes is around 60 m in engineering practice. However, due to the limitations of the available computational facility, $\frac{1}{10}$ of the practical conduit length is used in the present calculations for demonstration. Zone II comprises a cube with side length of $20D_h^*$ to ensure that its boundary conditions are reasonably specified by the ambient properties. The treatment of the interface of the two zones follows the overlapping grid method.[16] The dependent variables in the overlapping zone are transferred by the bilinear interpolation. The boundary conditions of zone II are as follows. On the surface of the inner cylinder, the same boundary conditions as specified for zone I are used. On the manhole surface, the no-slip condition and adiabatic wall are specified. The condition of zero normal gradient is met on the symmetric plane except for the normal velocity component, which vanishes naturally. On the free surfaces, the normal gradients of all of the dependent variables are set to be zero. The convergence criterion is described hereafter.

The general form of the discretized governing equations can be written as

$$A_P\Phi_P = \sum_{\text{nb}} A_{\text{nb}}\Phi_{\text{nb}} + b^\Phi \tag{10}$$

Define

$$B_i^\Phi = \left|A_P\Phi_P - \sum_{\text{nb}} A_{\text{nb}}\Phi_{\text{nb}} - b^\Phi\right| \tag{11}$$

$$H_i^\Phi = |A_P\Phi_P| + \left|\sum_{\text{nb}} A_{\text{nb}}\Phi_{\text{nb}} + b^\Phi\right| \tag{12}$$

$$\lambda^\Phi = \frac{\max\left(B_i^\Phi\right)}{(1/N)\sum_i H_i^\Phi} \tag{13}$$

where i is an arbitrary grid point in the computational domain and N is the total number of grid points. When $\lambda^\Phi \le 1.0\times10^{-4}$ for each dependent variable Φ in both of the zones, the iteration process is convergent.

Distribution of the grid nodes is arranged in such a way that the regions that have significant influences on the flowfield are adequately resolved. Illustration of the zonal grid distribution is schematically shown in Fig. 1. Numerical tests revealed that the maximum difference in mass inflow rate at the outlet plane between the $51\times51\times101$ (radial by angular by axial) and $61\times61\times121$ grid meshes for zone I, and the corresponding grid meshes for zone II are $21\times41\times21$ (x by y by z) and $31\times61\times31$, respectively, is less than 0.5%. Therefore, the former set of grid meshes is adopted in the present work.

Results and Discussion

To validate the computer model developed in this work, a benchmark problem of the three-dimensional natural convection in a differentially heated cubical enclosure,[25] which is schematically shown in Fig. 3, is first calculated for the case of $Ra = 10^5$ with a $51\times51\times26$ uniformly distributed grid mesh. The calculated result along the symmetric line ($y/L = 0.5$ and $z/L = 0.5$) is presented in Fig. 3 and compared with the result predicted by Fusegi et al.[25] Note that the Boussinesq approximation was made for the buoyancy term in Eq. (3) and that the energy dissipation term Φ in Eq. (5) was neglected in the calculation of Fusegi et al.[25] An excellent agreement

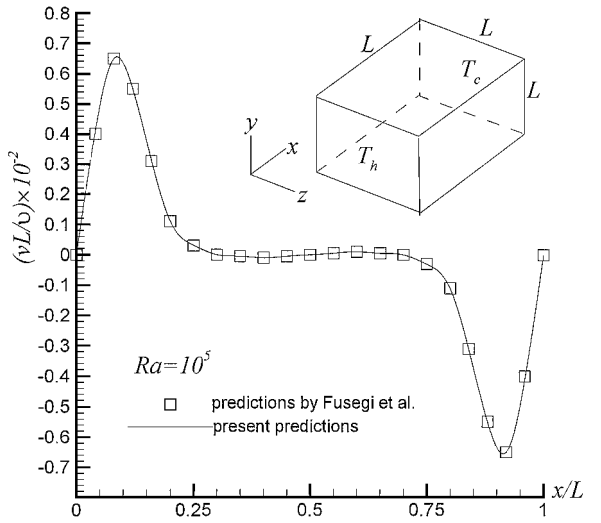

Fig. 3 Vertical velocity profile at the middle height in the symmetric plane ($y/L = 0.5$ and $z/L = 0.5$).

between the present calculation and the one obtained by Fusegi et al.[25] supports the validation of the developed computer model.

Because the thermal boundary conditions at the walls are specified in terms of heat fluxes instead of temperatures in the present work, a modified Rayleigh number is defined as follows:

$$Ra^0 = \frac{g^*\beta^*_{\text{ref}} D^{*3}_h}{\upsilon^*_{\text{ref}}\alpha^*_{\text{ref}}} \frac{q^*_w D^*_h}{k^*_{\text{ref}}} \tag{14}$$

As pointed out by Kuehn and Goldstein,[7] an onset of transition from laminar to turbulent regimes starts near $Ra = 4 \times 10^6$ for gases in a concentric annulus of $D_o/D_i = 2.6$. Moreover, a recent study by Labonia and Guj[9] indicated that chaotic flows were observed in the range of $0.9 \times 10^5 \le Ra \le 3.37 \times 10^5$ for a concentric annulus of $D_o/D_i = 2.36$. However, their conclusions were drawn from the experimental observations and based on the cases associated with the constant temperature differences between the outer and inner cylinders. Yoo[26] studied numerically the natural convection in a two-dimensional, narrow ($D_o/D_i = \frac{7}{6}$), horizontal, concentric annulus in the range of $0.001 \le Pr \le 0.3$ and $Gr \le 5 \times 10^4$. It is concluded that, for $Pr \le 0.2$, hydrodynamic instability induces steady or oscillatory flows consisting of multiple like-rotating cells, whereas thermal instability creates a counter-rotating cell on the top of annulus at $Pr = 0.3$. Kumar[5] made a numerical investigation using a two-dimensional model for an infinitely long, horizontal, concentric annulus where the inner cylinder was specified by a constant

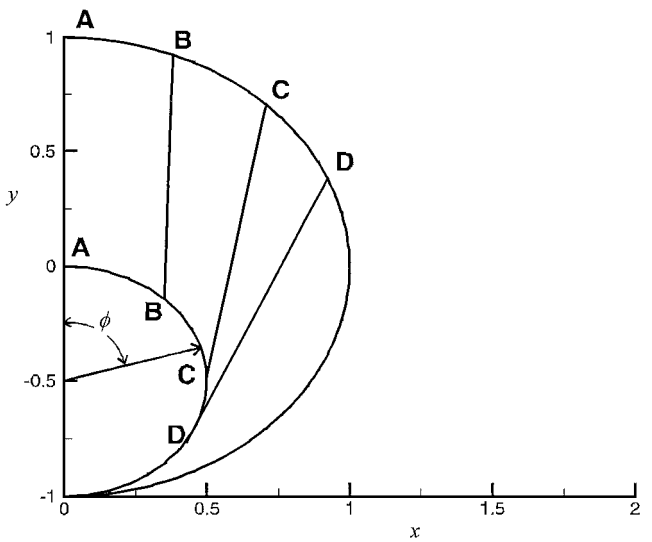

Transverse

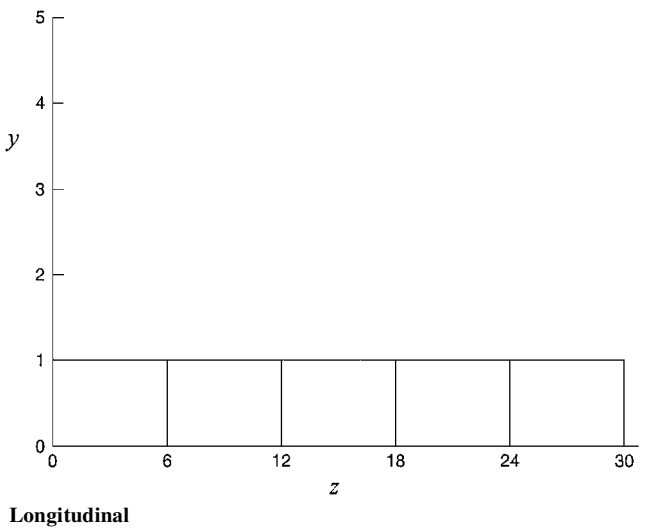

Longitudinal

Fig. 4 Illustration of the selected sections.

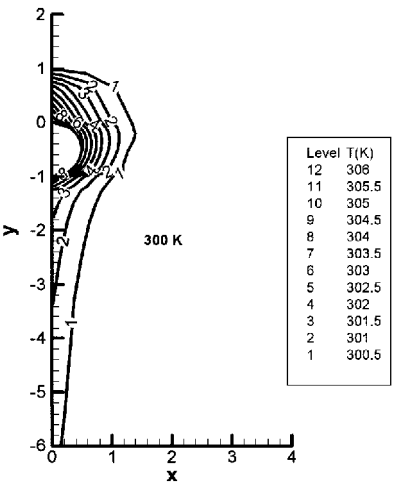

Fig. 5 Temperature contour near the end of the annulus ($z = 30.6$ and $Ra^0 = 10^6$).

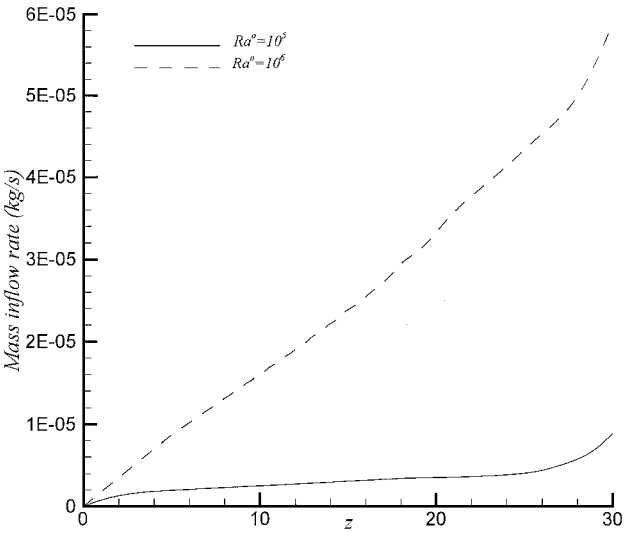

Fig. 6 Axial distributions of mass inflow rate.

$Ra^o = 10^5$

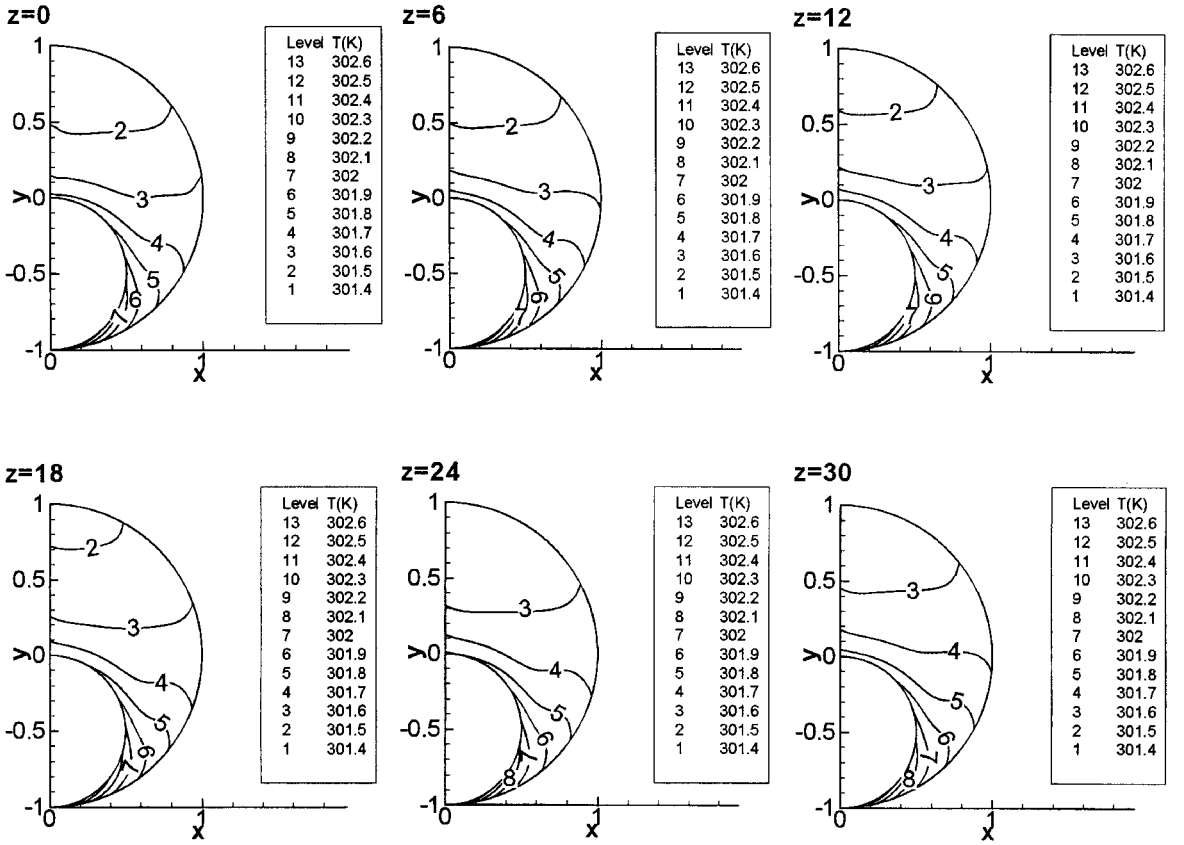

$Ra^o = 10^6$

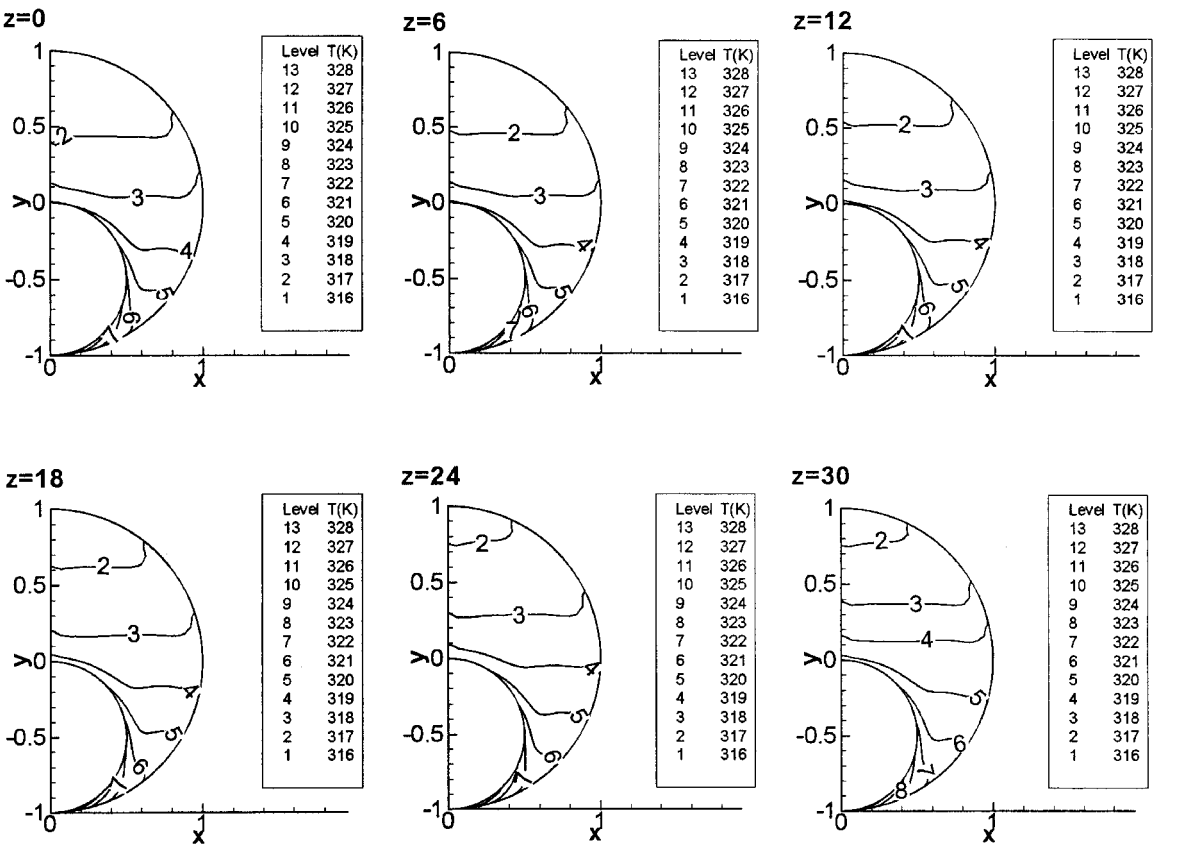

Fig. 7 Temperature contours at six transverse sections.

heat flux and the outer cylinder was isothermally cooled. He found that the critical modified Rayleigh numbers above which the numerical results failed to converge were 3.1×10^5 and 3×10^6 at $D_o/D_i = 1.5$ and 2.6, respectively. Kumar[5] also recognized that it was hard to judge whether the flow would become oscillatory or three-dimensional beyond the critical modified Rayleigh number for a given ratio of D_o/D_i. The present work, which is essentially a three-dimensional problem with the medium of air ($Pr = 0.7$), encounters the same convergence difficulty beyond $Ra^0 = \mathcal{O}(10^7)$, which may imply an onset of transition from steady laminar to chaotic or even turbulent flows. However, this issue is beyond the scope of this work and remains to be studied further. Here, two cases of $Ra^0 = 10^5$ and 10^6 are studied for demonstration.

Figure 2 shows the velocity vector plots at four selected longitudinal sections (see Fig. 4 for the section positions) for $Ra^0 = 10^5$ and 10^6. The result reveals that the ambient air is induced inward through the lower portion, whereas it flows outward through the upper portion of the conduit. This can also be observed from the temperature contour near the end of the annulus in zone II, as shown in Fig. 5. The mass inflow rate induced by natural convection is much larger for the case of $Ra^0 = 10^6$ than for $Ra^0 = 10^5$, as is clearly shown in Fig. 6. The steeper gradients of the mass inflow rates at the outlet of the conduit disclose that the zero-gradient type of fully developed outflow boundary conditions is not applicable to the problem investigated here. This observation corroborates the necessary use of an extended computational domain to the ambient environment, the zonal grid approach, in the present calculations.

Figure 7 displays the temperature contours at six selected transverse sections (see Fig. 4 for the section positions) with $Ra^0 = 10^5$ and 10^6. From the results shown in the downstream stations of Fig. 7, it is observed that the warmer air enters the lower portion, whereas the cooler air leaves through the upper portion of the conduit. Figure 5, which presents the temperature contour at the distance slightly outside the open end, that is, in zone II, corroborates the preceding observation. It is also observed that the highest temperatures occur near the bottom of the cable, where the power cable contacts the concrete conduit. Typical temperature profiles along the cable surface at six selected transverse sections for $Ra^0 = 10^5$ and 10^6 are presented in Fig. 8. It is clearly shown that the highest temperature in each transverse section is located right at the contacting point of the cable and the concrete conduit, that is, $\phi = 180$ deg. It is then concluded that the contacting point of the cable will deteriorate earliest. To figure out why the higher temperatures in each transverse section occur in the lower portion of the cable conduit, the azimuthal distributions of the local Rayleigh number Ra_l, at four selective transverse sections (see Fig. 4 for the section positions) for the two investigated cases are presented in Fig. 9. The local Rayleigh number Ra_l is defined by

$$Ra_l(\phi, z) = \frac{g^* \beta^*_{\text{ref}} \left[T_i^*(\phi, z) - T_o^*(\phi, z) \right] l^{*3}}{\upsilon^*_{\text{ref}} \alpha^*_{\text{ref}}} \tag{15}$$

where l^* is the radial distance between the inner (cable) and the outer (concrete conduit) surfaces, with the pole at the center of the inner

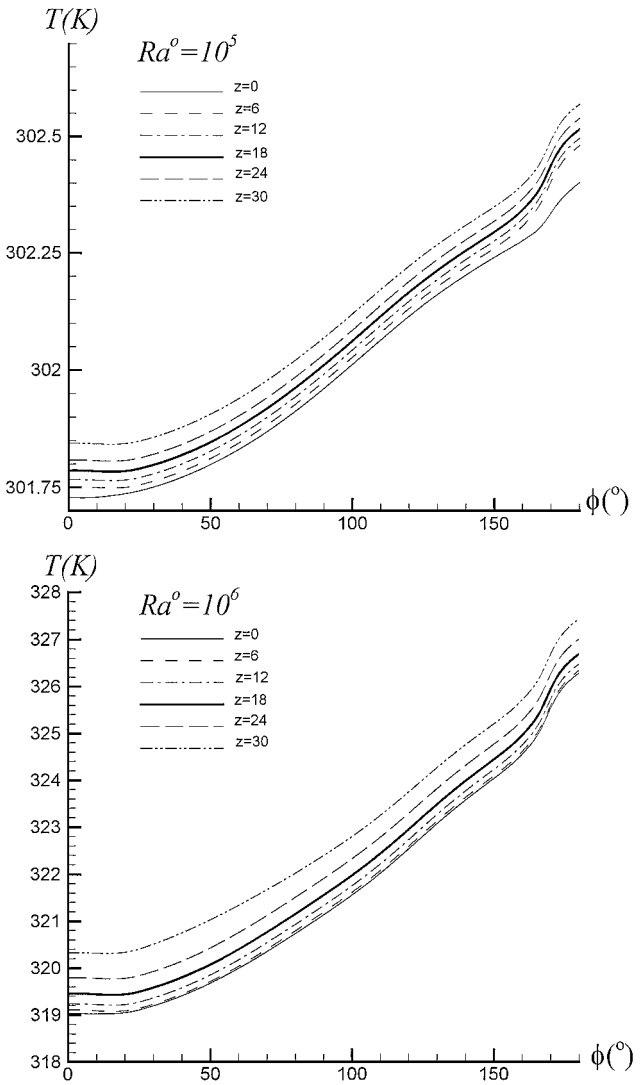

Fig. 8 Cable surface temperature distributions at six transverse sections.

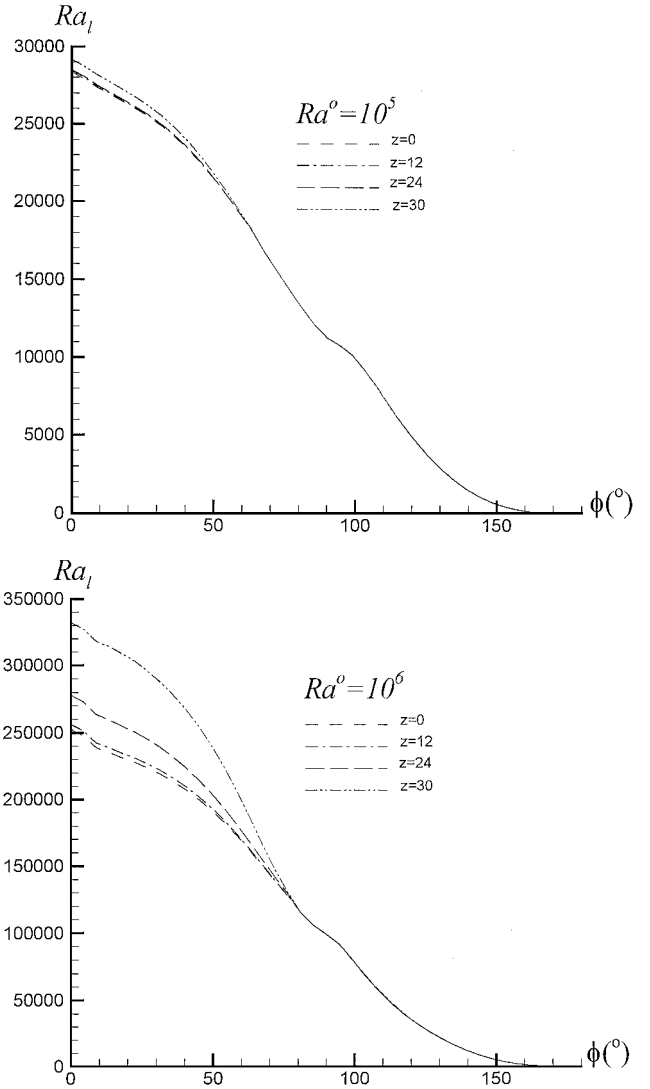

Fig. 9 Azimuthal distribution of the local Rayleigh numbers at four transverse sections.

cylinder, at a given azimuthal angle ϕ and longitudinal position z. Obviously, the l^* value approaches zero as ϕ moves to 180 deg, which corresponds to the contacting point of the cable and conduit. The definition of Ra_l ($Ra_l \propto l^{*3}$) leads to the results as shown in Fig. 9; that is, the local Rayleigh number drops steeply to zero value as ϕ increases to 180 deg. By definition, the Rayleigh number is equal to the Grashof number times the Prandtl number. Here the Grashof number provides a measure of the ratio of the buoyancy force to the viscous force acting on the fluid, that is, the air. Thus, at small local Rayleigh numbers the local heat transfer is mainly by conduction. As reported by Kuehn and Goldstein,[4] for the concentric annulus with $D_o/D_i = 2$ and with air, the heat transfer inside the annulus is dominated by conduction as $Ra_l \leq \mathcal{O}(10^3)$. Based on the preceding analysis, enhancement of the heat dissipation rate due to the natural convection effect vanishes near the bottom of the cable, and this leads to the results as disclosed in Figs. 5 and 8.

The result shown in Fig. 8 also reveals a trend that the cable (inner) surface temperature increases toward the outlet plane. This trend can also be deduced from a macroscopic energy balance of the cable conduit. Considering a control volume confined by the longitudinally symmetric plane ($z = 0$), the outer (concrete conduit) and inner (cable) cylinders, and a specified axial section (for example, at the position z), the outflow air has to carry away more heat as z increases because the total heat dissipated from the cable to the control volume is proportional to z. In the two cases investigated, the calculated maximum temperature increments on the cable surface are about 2.7 and 27.5 K for $Ra^0 = 10^5$ and 10^6, respectively.

Figure 10 compares the averaged Nusselt number distributions on the cable surface for $Ra^0 = 10^5$ and 10^6. Here the averaged Nusselt number is defined by

$$\overline{Nu}(z) = \frac{1}{\pi}\int_0^{\pi} Nu(\phi, z)\, \mathrm{d}\phi \tag{16}$$

with

$$Nu(\phi, z) = 1/[\theta_w(\phi, z) - \theta_b(z)] \tag{17}$$

where the bulk temperature is calculated by[27]

$$\theta_b(z) = \frac{\oint\!\!\oint_A \theta(r, \phi, z)\rho|\boldsymbol{V}\cdot \mathrm{d}\boldsymbol{A}|}{\oint\!\!\oint_A \rho|\boldsymbol{V}\cdot \mathrm{d}\boldsymbol{A}|} \tag{18}$$

Note that the Nusselt number defined on the outer (concrete conduit) surface is identically zero due to the specified adiabatic boundary condition. Figure 10 shows that both $\overline{Nu}$ curves decrease toward the outlet plane for the two cases. It also highlights a three-dimensional nature in the present problem, particularly for the condition at large modified Rayleigh numbers.

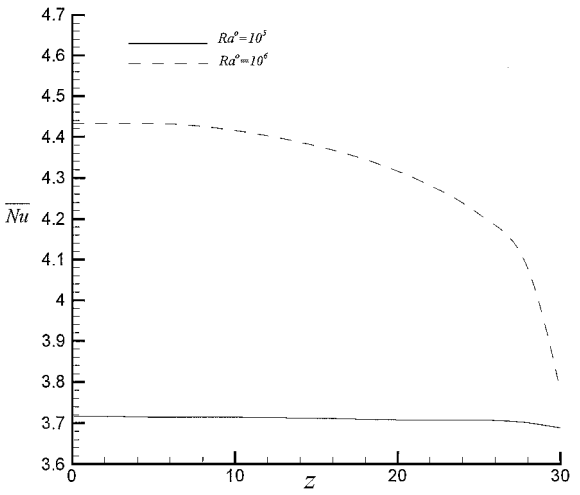

Fig. 10 Axial distributions of Nusselt number on the inner cylinder.

Conclusions

Three-dimensional natural convection between horizontal, highly eccentric cylinders, which simulates the heat dissipation process occurring within power cable conduits buried underground, is numerically analyzed. Two cases with $Ra^0 = 10^5$ and 10^6 are investigated. It is found that cable surface temperature increases toward the outlet plane. In addition, the highest temperature occurs at the bottom of the inner cylinder (cable), where the power cable contacts the concrete conduit (outer cylinder), in each transverse section for both cases. A study on the azimuthal distribution of the local Rayleigh number Ra_l, in which the characteristic length is defined in terms of radial distance between the inner and outer cylinders, in each transverse section reveals that the local Rayleigh number drops steeply to zero value as ϕ approaches 180 deg (the contacting point). At small local Rayleigh numbers the local heat transfer is mainly by conduction, but not by natural convection. This explains why the higher temperatures occur in the flow region near the bottom of the inner cylinder. It is also observed that the azimuthally averaged Nusselt number decreases from the longitudinally symmetric plane ($z = 0$) toward the outlet plane.

Acknowledgment

The authors wish to acknowledge the support from the National Science Council, Republic of China, under Grant NSC88-2213-E-150-003.

References

[1]El-Shaarawi, M. A. I., and Mokheimer, E. M. A., "Free Convection in Vertical Eccentric Annuli with a Uniformly Heated Boundary," *International Journal for Numerical Methods in Heat and Fluid Flow*, Vol. 8, No. 5, 1998, pp. 488–503.

[2]Ho, C. J., and Lin, Y. H., "Natural Convection Heat Transfer of Cold Water Within an Eccentric Horizontal Cylindrical Annulus," *Journal of Heat Transfer*, Vol. 110, No. 4, 1988, pp. 894–900.

[3]Prusa, J., and Yao, L. S., "Natural Convection Heat Transfer Between Eccentric Horizontal Cylinders," *Journal of Heat Transfer*, Vol. 105, No. 1, 1983, pp. 108–116.

[4]Kuehn, T. H., and Goldstein, R. J., "Correlating Equations for Natural Convection Heat Transfer Between Horizontal Circular Cylinders," *International Journal of Heat and Mass Transfer*, Vol. 19, No. 10, 1976, pp. 1127–1134.

[5]Kumar, R., "Study of Natural Convection in Horizontal Annuli," *International Journal of Heat and Mass Transfer*, Vol. 31, No. 6, 1988, pp. 1137–1148.

[6]Guj, G., Iannetta, S., and Moretti, G., "Experimental Analysis of Thermal Fields in Horizontally Eccentric Cylindrical Annuli," *Experiments in Fluids*, Vol. 12, No. 6, 1992, pp. 385–393.

[7]Kuehn, T. H., and Goldstein R. J., "An Experimental Study of Natural Convection Heat Transfer in Concentric and Eccentric Horizontal Cylindrical Annuli," *Journal of Heat Transfer*, Vol. 100, No. 4, 1978, pp. 635–640.

[8]Kuehn, T. H., and Goldstein R. J., "An Experimental and Theoretical Study of Natural Convection in the Annulus Between Horizontal Concentric Cylinders," *Journal of Fluid Mechanics*, Vol. 74, Pt. 4, April 1976, pp. 695–719.

[9]Labonia, G., and Guj, G., "Natural Convection in a Horizontal Concentric Cylindrical Annulus: Oscillatory Flow and Transition to Chaos," *Journal of Fluid Mechanics*, Vol. 375, Nov. 1998, pp. 179–202.

[10]Moukalled, F., and Acharya, S., "Natural Convection in the Annulus Between Concentric Horizontal Circular and Square Cylinders," *Journal of Thermophysics and Heat Transfer*, Vol. 10, No. 3, 1996, pp. 524–531.

[11]Glakpe, E. K., Watkins, C. B., Jr., and Cannon, J. N., "Constant Heat Flux Solutions for Natural Convection Between Concentric and Eccentric Horizontal Cylinders," *Numerical Heat Transfer*, Vol. 10, No. 3, 1986, pp. 279–295.

[12]Iyer, S. V., and Vafai, K., "Buoyancy Induced Flow and Heat Transfer in a Cylindrical Annulus with Multiple Perturbations," *International Journal of Heat and Mass Transfer*, Vol. 41, No. 20, 1998, pp. 3025–3035.

[13]Iyer, S. V., and Vafai, K., "Effects of a Geometric Perturbation on Buoyancy Induced Flow and Heat Transfer in a Cylindrical Annulus," *International Journal of Heat and Mass Transfer*, Vol. 40, No. 12, 1997, pp. 2901–2911.

[14]Desai, C. P., and Vafai, K., "An Investigation and Comparative Analysis of Two- and Three-Dimensional Turbulent Natural Convection in a Horizontal Annulus," *International Journal of Heat and Mass Transfer*, Vol. 37, No. 16, 1994, pp. 2475–2504.

[15] Vafai, K., and Ettefagh, J., "An Investigation of Transient Three-Dimensional Buoyancy-Driven Flow and Heat Transfer in a Closed Horizontal Annulus," *International Journal of Heat and Mass Transfer*, Vol. 34, No. 10, 1991, pp. 2555–2569.

[16] Rai, M. M., "Navier–Stokes Simulations of Rotor–Stator Interaction Using Patched and Overlaid Grids," AIAA Paper 85-1519, 1985.

[17] Lee, D., and Yeh, C. L., "Computation of Reacting Flame Stabilizer Flows Using a Zonal Grid Method," *Numerical Heat Transfer*, Pt. A, Vol. 24, No. 3, 1993, pp. 273–285.

[18] Vafai, K., and Ettefagh, J., "The Effects of Sharp Corners on Buoyancy-Driven Flows with Particular Emphasis on Outer Boundaries," *International Journal of Heat and Mass Transfer*, Vol. 33, No. 10, 1990, pp. 2311–2328.

[19] Vafai, K., and Ettefagh, J., "Thermal and Fluid Flow Instabilities in Buoyancy-Driven Flows in Open-Ended Cavities," *International Journal of Heat and Mass Transfer*, Vol. 33, No. 10, 1990, pp. 2329–2344.

[20] Chang, T. S., and Lin, T. F., "On the Reversed Flow and Oscillating Wake in an Asymmetrically Heated Channel," *International Journal for Numerical Methods in Fluids*, Vol. 10, No. 4, 1990, pp. 443–459.

[21] Choudhury, D., and Patankar, S. V., "Combined Forced and Free Laminar Convection in the Entrance Region of an Inclined Isothermal Tube," *Journal of Heat Transfer*, Vol. 110, No. 4, 1988, pp. 901–909.

[22] Thompson, J. F., Warsi, Z. U. A., and Mastin, C. W., "Elliptic Generation Systems," *Numerical Grid Generation*, North-Holland, Amsterdam, 1985, pp. 188–271.

[23] Van Doormaal, J. P., and Raithby, G. D., "Enhancements of the SIMPLE Method for Predicting Incompressible Fluid Flows," *Numerical Heat Transfer*, Vol. 7, No. 2, 1984, pp. 147–163.

[24] Hayase, T., Humphrey, J. A. C., and Grief, R., "A Consistently Formulated QUICK Scheme for Fast and Stable Convergence Using Finite-Volume Iterative Calculation Procedures," *Journal of Computational Physics*, Vol. 98, No. 1, 1992, pp. 108–118.

[25] Fusegi, T., Hyun, J. M., Kuwahara, K., and Farouk, B., "A Numerical Study of Three-Dimensional Natural Convection in a Differentially Heated Cubical Enclosure," *International Journal of Heat and Mass Transfer*, Vol. 34, No. 6, 1991, pp. 1543–1557.

[26] Yoo, J. S., "Natural Convection in a Narrow Horizontal Cylindrical Annulus: $Pr \leq 0.3$," *International Journal of Heat and Mass Transfer*, Vol. 41, No. 20, 1998, pp. 3055–3073.

[27] Patankar, S. V., Liu, C. H., and Sparrow, E. M., "Fully Developed Flow and Heat Transfer in Ducts Having Streamwise-Periodic Variations of Cross-Sectional Area," *Journal of Heat Transfer*, Vol. 99, No. 2, 1977, pp. 180–186.